

Article

Separation of Carbon Dioxide from Real Power Plant Flue Gases by Gas Permeation Using a Supported Ionic Liquid Membrane: An Investigation of Membrane Stability

Patrik Klingberg ^{1,*}, Kai Wilkner ², Markus Schlüter ^{1,†}, Judith Grünauer ^{1,‡}
and Sergey Shishatskiy ¹

¹ Helmholtz-Zentrum Geesthacht, Institute of Polymer Research, Max-Planck-Straße 1, 21502 Geesthacht, Germany; markus.schluter@preussenelektra.de (M.S.); judith.gruenauer@tesa.com (J.G.); sergey.shishatskiy@hzg.de (S.S.)

² Forschungszentrum Jülich GmbH, Institute of Energy and Climate Research, IEK-1: Materials Synthesis and Processing, D-52425 Jülich, Germany; k.wilkner@fz-juelich.de

* Correspondence: patrik.klingberg@hzg.de; Tel.: +49-4152-87-2495

† Current address: PreussenElektra GmbH, Kernkraftwerk Brokdorf, 25576 Brokdorf; Germany.

‡ Current address: tesa SE, Hugo-Kirchberg-Strasse 1, 22848 Norderstedt, Germany.

Received: 3 January 2019; Accepted: 15 February 2019; Published: 4 March 2019



Abstract: The separation of carbon dioxide from coal-fired power plant flue gases using a CO₂/N₂-selective supported ionic liquid membrane (SILM) was investigated and the performance and stability of the membrane during operation are reported. The membrane is composed of a polyacrylonitrile (PAN) ultrafiltration membrane as a support and a selective layer of an ionic liquid (IL), 1-ethyl-3-methylimidazolium bis(trifluoromethylsulfonyl)imide (EMIM Tf₂N). The feasibility of large-scale SILM production was demonstrated by the formation of a square-meter-scale membrane and preparation of a membrane module. A flat-sheet envelope-type SILM module containing 0.67 m² of the membrane was assembled. Prior to real flue gas operation, the separation behaviour of the membrane was investigated with single gases. The stability of the SILM during the test stand and pilot plant operation using real power plant flue gases is reported. The volume fraction of carbon dioxide in the flue gas was raised from approx. 14 vol. % (feed) to 40 vol. % (permeate). However, issues concerning the membrane stability were found when SO₃ aerosols in large quantities were present in the flue gas.

Keywords: supported ionic liquid membrane; gas permeation; coal-fired power plant flue gas; CO₂ separation; SO₃ aerosols

1. Introduction

CO₂ is a greenhouse gas with a significant impact on climate change [1] and a large amount of CO₂ is emitted to the environment by power plant flue gases. It is very probable that, despite the high risk of global warming, the number of coal-fired power plants in countries with large coal reserves, such as China and the United States of America, will increase in the future [2]. In Germany, the percentage of renewable energies increased from 6% to 29% during the 2000–2017 period [3]. Nevertheless, it is likely that fossil fuel-fired power plants will remain necessary in Germany for many years to ensure a continuous, non-fluctuating energy supply.

Carbon Capture (CC) technologies afford opportunities to make power plants more climate-friendly [4–6]. Gas permeation is one possibility for CC and membranes have several

advantages compared with competing processes, for example, amine absorption [7]. Membranes are more load flexible, meaning that they can better deal with changing flue gas compositions. Another argument in favour of gas permeation is the short response time of membranes. This feature makes gas permeation very interesting as a method of CC from flue gases generated by German power plants because, nowadays, some plants start up and shut down several times a year, while others often ramp down into partial-load operation. For high degrees of CO₂ separation, large membrane areas are required but the separation of CO₂ from only a fraction of flue gas streams could still be useful since the purified CO₂ may be used as a feedstock in the chemical industry [8].

Research in the area of CO₂ separation from gaseous mixtures using gas permeation processes has been attracting increasing attention since the invention of membranes with high CO₂/N₂ selectivities ($\alpha_{\text{CO}_2/\text{N}_2}$ up to 50 at $\vartheta = 30$ °C) and high CO₂ permeances (L_{CO_2} up to 6 m³(STP)/(m²·h·bar) at $\vartheta = 30$ °C). These membranes are mainly thin-film composite membranes (TFCMs) with selective layers out of poly(ethylene oxide) (PEO)-containing polymers. One example is a TFCM with a selective layer of PolyActive™ 1500—a commercially available polymer that is based on a poly(ethylene oxide)–poly(butylene terephthalate) (PEO–PBT) block copolymer [9]. Another example is a TFCM with the block copolymer Pebax®MH 1657 (poly(ether-b-amide-6)) [10]. Pebax® has a higher CO₂/N₂ selectivity but lower CO₂ permeance than PolyActive™ 1500 at 30 °C [9]. Also, the second-generation Polaris™ membrane from Membrane Technology and Research, Inc. (MTR) [11], should be mentioned, as it has separation properties comparable to those of the PolyActive™ 1500 TFCM.

Other materials with promising CO₂/N₂ separation properties are ionic liquids (ILs). Research in the field of ILs, which are commonly defined as salts with melting points below 100 °C [12], was first published in 1914 by Paul Walden [13]. ILs have properties that make them interesting candidates for the design of new membranes. An important feature of ILs is that they are exceptionally chemically tuneable. An extensive variety of ILs with task-specific properties are currently available. The combination of properties like negligible volatility [14], thermal stability [15], low flammability [16] and high ionic conductivity [17] makes ILs exceptionally interesting for various applications.

In previous studies, our group investigated three commercially available imidazole-based room-temperature ILs with promising CO₂/N₂ separation properties [18,19] as potential materials for the selective layer of gas separation membranes. 1-Ethyl-3-methylimidazolium dicyanoamide (EMIM DCA) has an attractive ideal selectivity ($\alpha_{\text{CO}_2/\text{N}_2}$ up to 55 at $\vartheta = 30$ °C). 1-Ethyl-3-methylimidazolium bis(trifluoromethylsulfonyl)imide (EMIM Tf₂N) has an ideal CO₂/N₂ selectivity of 30 at $\vartheta = 30$ °C. We can see from these examples that the selectivity of some ILs is in the range of values considered characteristic of PEO-containing polymers and the fact that the CO₂ permeabilities of these ILs [19] exceed those of the aforementioned polymers makes ILs even more appealing candidates for membrane development. Nevertheless, there remains a challenge to develop stable, large-scale (re)producibile IL-membranes whose selective IL layer thickness is close to that of PEO-containing polymer membranes.

In recent years, various IL-based membranes for CO₂ separation have been developed and investigated. Tomé et al. discussed different configurations of IL-based CO₂ separation membranes from a material engineering point of view [20]. There are several different membrane configurations: supported ionic liquid membranes (SILMs), polymer/IL composite membranes, gelled IL membranes and polymerized ionic liquid (PIL) membranes. Zhou et al. successfully developed a TFCM that was prepared from a room-temperature IL/polymerized (room-temperature IL) composite material [21]. The membrane showed an excellent CO₂ permeance of 6100 ± 400 GPU (1000 GPU = 2.7 m³(STP)/(m²·h·bar)) and a good CO₂/N₂ selectivity of 22 ± 2.

However, besides good separation properties, the mechanical and chemical stability of a membrane is also crucial for realizing a long membrane lifetime despite operating in the hazardous environment of a power plant flue gas. An overview of IL-based CO₂ separation membranes, with a focus on the membrane engineering perspective, was given by Dai et al. [22]. In addition, Wang et al. [23] discussed the chemical stability of ILs. However, to our knowledge, a practical demonstration

of whether IL-containing membranes remain stable during their operation in real power plant flue gas has not been reported until now.

To our knowledge, in this paper, the stability of an SILM during the separation of CO₂ from power plant flue gas is reported for the first time. The SILM used in the study is composed of a polyacrylonitrile (PAN) ultrafiltration membrane as a support and EMIM Tf₂N as the IL, which provides the membrane with the selectivity property. This paper reports the preparation of various SILMs that differ in the morphology of the PAN support and the composition of the IL coating solution used for preparation; the results of the experiments are then discussed. The large-scale preparation of the SILM which showed the most promising separation performance after a small-scale preparation is reported. Furthermore, flat-sheet SILM envelopes and a flat-sheet envelope-type SILM module with a membrane area of 0.67 m² were fabricated and the quality control results for each step of the preparation are reported. The membrane separation performance of the SILM for each step of preparation (from SILM sheet to SILM module) was therefore tested with single gases.

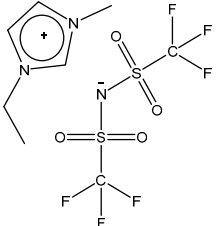
However, the main focus of our research was the investigation of the SILM's stability during power plant flue gas operation. First, the stability of the SILM was investigated using a gas permeation test stand located at the lignite-fired power plant (block K) of RWE Power AG in Niederaussem, Germany. Second, the SILM module was installed in a gas permeation pilot plant that is located at the hard coal-fired Rheinhafen Dampfkraftwerk in Karlsruhe (block 8) of EnBW AG in Karlsruhe, Germany, where stability investigations were conducted during real flue gas operation.

2. Materials and Methods

2.1. Membrane Materials

The ionic liquid (Table 1) 1-ethyl-3-methylimidazolium bis(trifluoromethylsulfonyl)imide, solvents and other chemicals for SILM production were purchased from Sigma-Aldrich Chemie GmbH, Munich, Germany. The chemicals were not further modified before use.

Table 1. Ionic liquid used in this study and its physical properties.

Abbreviation	Structure	Molecular Mass [g/mol]	Viscosity at 25 °C [mPa·s]	Density at 25 °C [kg/m ³]
EMIM Tf ₂ N		391.3	32 [24]	1518 [25]

Polyacrylonitrile (PAN) ultrafiltration membranes [26] were produced in-house by the phase inversion process. The PAN porous membranes used as a support for the SILMs were all prepared from PAN–organic solvent solutions using a PAN concentration of 13.4 wt. %. Two different solvent mixtures were used (1 and 2). The composition of the PAN solution in organic solvent, which was used for porous membrane preparation, cannot be disclosed due to the licensing limitations. In addition, the gap width between the doctor blade and nonwoven material during PAN membrane preparation was varied for M1 and M2, each of which had three different variants (a–c). Thus, in total, six PAN membranes (M1a–M1c and M2a–M2c) with different porous layer thicknesses and total porosities were prepared (Table 2 and Figure 1).

Table 2. Polyacrylonitrile (PAN) membranes used as support for supported ionic liquid membranes (SILMs): differences in preparation conditions and resulting porous layer thickness.

PAN Membrane	Solvent Variant	Doctor Blade Gap Width [μm]	PAN Thickness [μm]
M1a	1	150	28.3
M1b	1	170	28.8
M1c	1	200	30.6
M2a	2	150	21.3
M2b	2	170	21.6
M2c	2	200	22.6

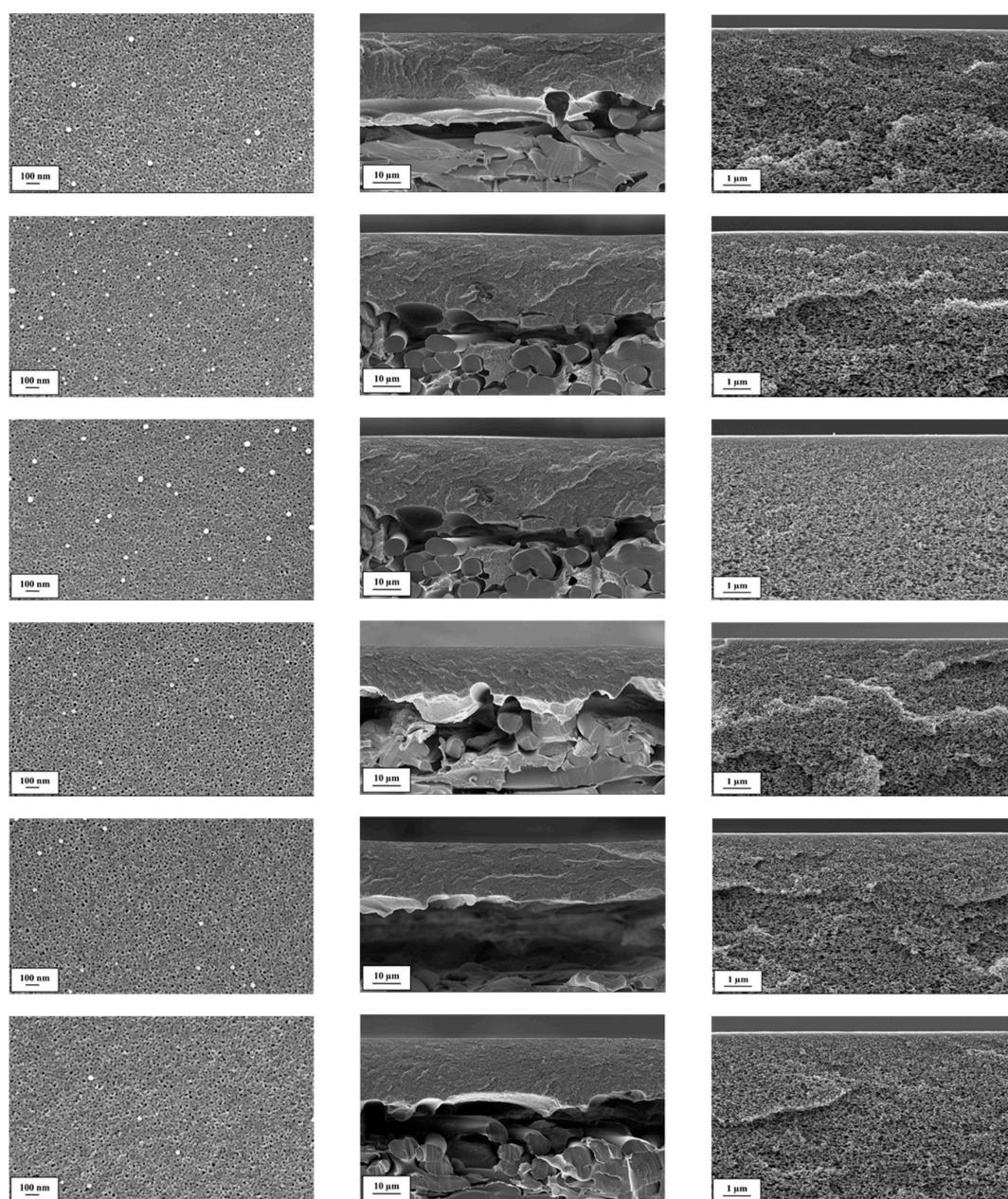


Figure 1. Scanning electron microscope (SEM) images of PAN membranes M1a, M1b, M1c, M2a, M2b and M2c (top to bottom) of (left) membrane surface, (middle) membrane cross-section and (right) membrane cross-section at higher magnification.

2.2. Supported Ionic Liquid Membrane Preparation

This study involved the preparation and characterization of twelve SILMs to investigate the influence of the support structure and the coating solution composition on the membrane performance. The membranes were prepared on PAN ultrafiltration membranes, which were used as the porous support and have proved to be suitable for scalable coating techniques [19]. The support membranes M1a–M1c and M2a–M2c (Figure 1) were coated with two different coating solutions (15 wt. % and 20 wt. % IL in methanol), resulting in twelve SILMs: M1a15–M1c15, M1a20–M1c20, M2a15–M2c15 and M2a20–M2c20. The membranes were prepared with a pilot-scale dip and roller coating machine, which is used in-house for the fabrication of various TFCMs [9,27,28]. Membranes with a length of up to 250 m and a coating width of up to 0.61 m can be prepared. Small-scale dip coating of a porous substrate with an IL–methanol solution was previously described by our group [19]. In contrast to the preparation in the aforementioned study, the preparation in the current study was done without a pore-blocking liquid. During the coating process, the coating solution was applied to the porous support by creating a meniscus between the coating roll and the support, as shown in Figure 2. In the region where the support contacts the coating solution meniscus, both the IL and solvent penetrate the porous support due to capillary force. Immediately after leaving the meniscus, the volatile solvent starts to evaporate and is then forced to evaporate further in a pre-dryer and main-dryer, which are both integrated into the coating machine.

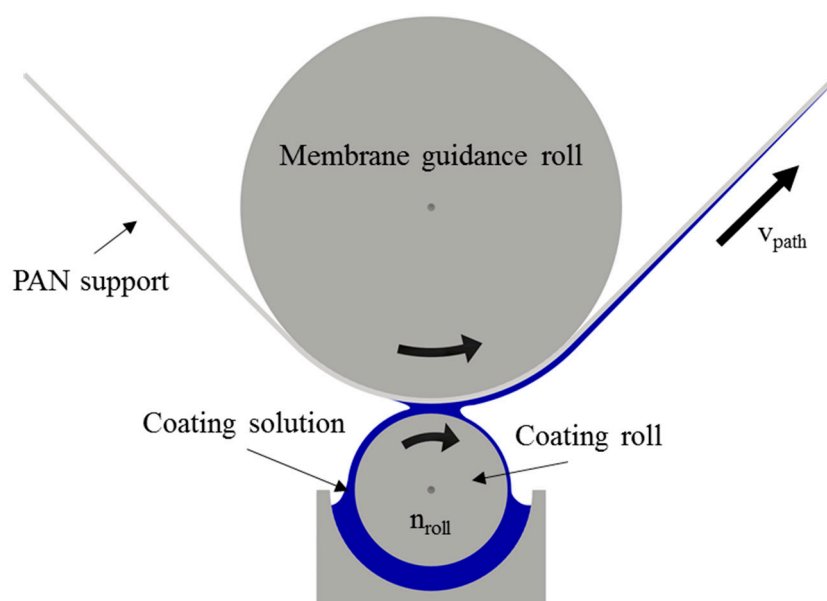


Figure 2. Drawing of the two-roll system of the large-scale dip and roller coating machine. Meniscus formation between the PAN support and coating roll.

The speed of the coating roll n_{roll} was adjusted to a maximum value of 10 min^{-1} in order to prevent meniscus damage due to the low viscosities of the coating solutions. The membrane was automatically dragged through the coating machine with a constant path velocity of $v_{\text{path}} = 0.31 \text{ m/s}$. A main-dryer temperature of $60 \text{ }^\circ\text{C}$ was chosen to reliably evaporate the residual solvent.

2.3. Water Permeance Measurements

Pure water permeance measurements were taken to draw conclusions about the regularity of the morphology of the PAN support membranes M1a–M1c and M2a–M2c. The method of measuring water permeance was previously described by our group [19]. The pure water permeance of six circular membrane stamps of each PAN membrane was measured. The water permeance F is the volume V [L]

of the water permeating through the membrane with a membrane area A_{Mem} [m^2] during the time period Δt [h] at a pressure difference Δp [bar]:

$$F = \frac{V}{A_{\text{Mem}} \cdot \Delta t \cdot \Delta p}. \quad (1)$$

2.4. Determination of Single Gas Permeances and Selectivities

Single gas measurements were carried out in order to find the combination of the PAN support (M1a–M1c and M2a–M2c) and coating solution (15 wt.% and 20 wt.%) resulting in the best-performing SILM as judged by the CO_2 permeance and CO_2/N_2 selectivity. For single gas measurements, circular membrane stamps were located in a dead-end testing cell. Round stamps with a membrane area of $A_{\text{Mem}} = 0.00342 \text{ m}^2$ were collected from the initial and end parts of each produced SILM sheet (M1a15/20–M1c15/20 and M2a15/20–M2c15/20). The SILMs were impinged by a gauge pressure of $p_{\text{F},i} = 2 \text{ bar}$. The permeate pressure during measurements was atmospheric. The resulting steady-state permeate volume flow $\dot{V}_{\text{P},i}$ was measured with a Bios Defender 220 flow meter and the permeance L of component i was then calculated according to the following equation:

$$L_i = \frac{\dot{V}_{\text{P},i}}{A_{\text{Mem}} \cdot (p_{\text{R},i} - p_{\text{P},i})}, \quad (2)$$

where $p_{\text{R},i} = p_{\text{F},i}$ and ideal gas behaviour is assumed due to the low pressures applied. The ideal gas selectivity $\alpha_{i,j}$ is the ratio of the single gas permeances of components i and j :

$$\alpha_{i,j} = \frac{L_i}{L_j}. \quad (3)$$

Furthermore, single gas pressure increase measurements were done with an in-house developed automatic membrane gas transport property determination facility. The facility allows for the automatic determination of the membrane's gas separation performance for up to 15 gases by utilizing the constant volume/variable pressure method [29] for a feed pressure range of 100–1200 mbar and a temperature range of 5–120 °C. The permeances of O_2 , N_2 and CO_2 were determined for the membrane M1c15. In addition, the CO_2/N_2 and O_2/N_2 ideal selectivities were calculated.

2.5. Membrane Envelope Preparation and Testing

Double-sided envelopes of flat-sheet membranes with a diameter of 0.1 m and a total membrane area of 0.0114 m^2 were manufactured by the thermal welding of two membrane sheets, two nonwoven sheets and a permeate spacer sheet for each envelope. The sheets were prepared with a punch. The outsides of the membrane envelopes are formed by SILM sheets, with the selective layer outside (see Figure 3). The permeate spacer is located in the middle of the envelope to ensure a permeate channel with sufficient thickness during operation. In order to prevent membrane damage from the rough spacer, a nonwoven material is placed between the SILM sheet and the spacer on each side.

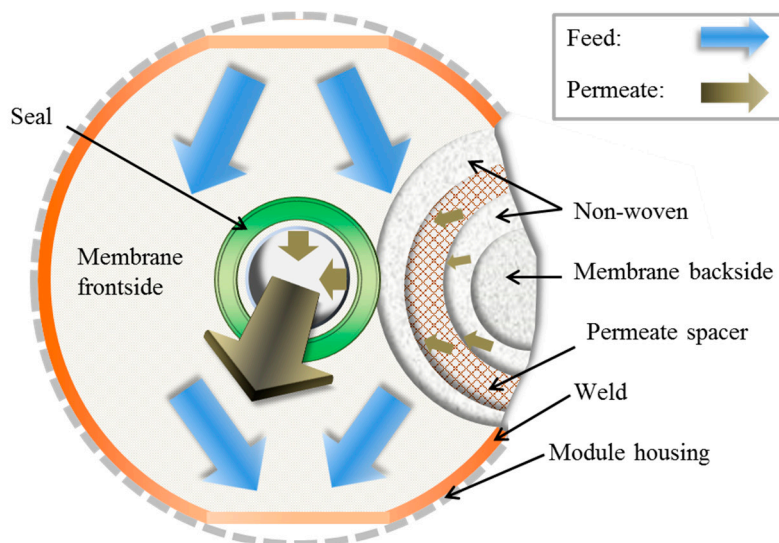


Figure 3. Drawing of membrane envelope with different layers with flow directions indicated.

Following the preparation, membrane envelope quality control testing was done with an in-house developed envelope-testing unit. With the envelope-testing unit, the permeances of the single gases (N_2 , O_2 and CO_2) were measured and CO_2/N_2 and O_2/N_2 selectivities were calculated for each envelope. Finally, membrane envelopes with an unsatisfactory permeance or selectivity were rejected and intact ones were integrated into module housing.

2.6. Module Preparation and Testing

An envelope-type [30–32] K100 flat-sheet module (membrane module with an inner diameter of 100 mm and maximum membrane area of 1 m^2 (see Figure 4) was prepared by installing 59 SILM envelopes for a total membrane area of 0.67 m^2 . After module preparation, the quality of the module was checked to exclude leaks that formed during module manufacturing. For quality control, the module was pressurized at a defined feed pressure with compressed air. The resulting permeate volume flow was measured with a Bios Defender 220 flow meter (Mesa Laboratories, Inc., Lakewood, CO, USA) and the oxygen volume fraction in the permeate was measured with a SICK Transic111LP oxygen meter (SICK AG, Waldkirch, Germany). The O_2 and N_2 permeances and O_2/N_2 selectivity then were calculated using Equation (2). To make a comparison, the permeance and selectivity determination was done again using the single gases (O_2 and N_2).

2.7. Investigation of SILM Stability during Real Power Plant Flue Gas Operation

To investigate the stability of the SILM during real power plant flue gas operation, the membranes were tested at two power plants. The first site was a gas permeation test stand located at the lignite-fired power plant Niederaussem (block K) of RWE Power AG, Bergheim, Germany. The second location was the hard coal-fired Rheinhafen-Dampfkraftwerk (block 8) of EnBW AG in Karlsruhe, Germany, where a gas permeation pilot plant operates.

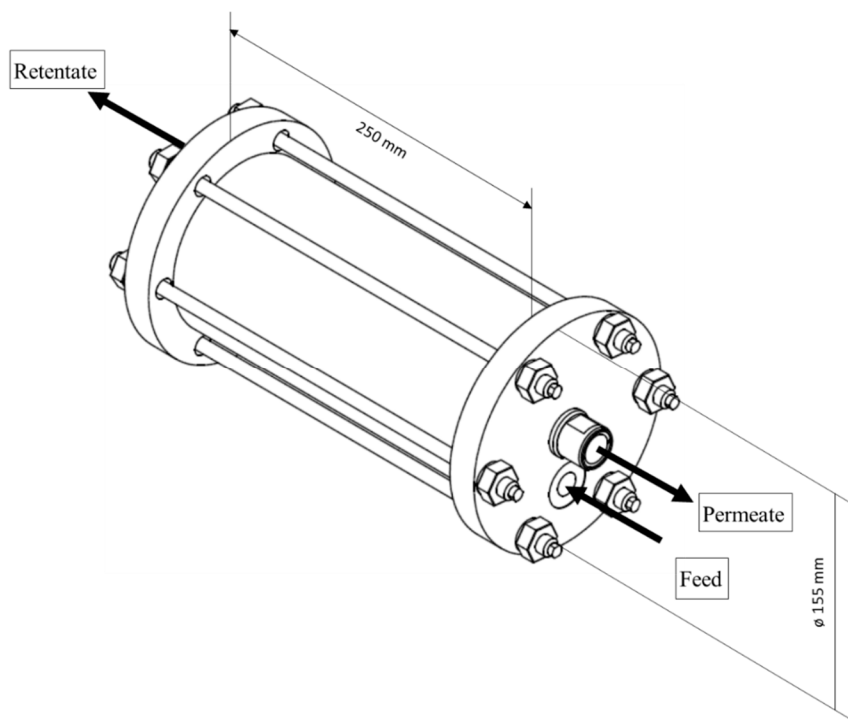


Figure 4. Schematic drawing of K100 envelope-type flat-sheet membrane module.

2.7.1. Gas Permeation Test Unit at Lignite-Fired Power Plant

The tests in the flue gas of the lignite-fired power plant were performed using a small-area membrane gas permeation test rig. This test rig was designed to test membrane samples with areas between 8 cm² and 50 cm² at temperatures between 40 °C and 70 °C and water content between 2% rH and 80% rH. The test stand can be used to conduct stability tests of membrane samples before building a large-area module. The test rig is located at RWE Power AG’s “Coal Innovation Centre” at the power plant Niederaussem in Germany and operated by the Forschungszentrum Jülich IEK-1. The test rig is installed downstream of a high-performance scrubber (FGDplus)—an optimized flue gas scrubbing pilot plant [33]. Figure 5 shows a simplified flowchart of the gas permeation test rig. Before entering the membrane test cell, the flue gas is cooled in K1 to a desired dew point temperature and superheated in K2 to the test temperature. By these pre-treatment steps, the relative humidity of the feed gas was defined as 35% relative humidity (dew point = 22 °C) and damage to the membrane material from condensation in the test cell should be avoided (see also 3.6.2). After the filter (F1), a feed pump (P1) was installed to overcome the feed-/retentate-side pressure drop and to adjust a constant feed volume flow. The feed volume flow during the SILM measurement campaign was about 0.12 m³(STP)/h and the feed pressure was about 1.06 bar. The feed temperature was kept nearly constant at $\vartheta_F \sim 40$ °C by trace heating the pipes and the heated test cell. The driving force was generated by a membrane vacuum pump (P2), which reduced the permeate pressure to 20 mbar.

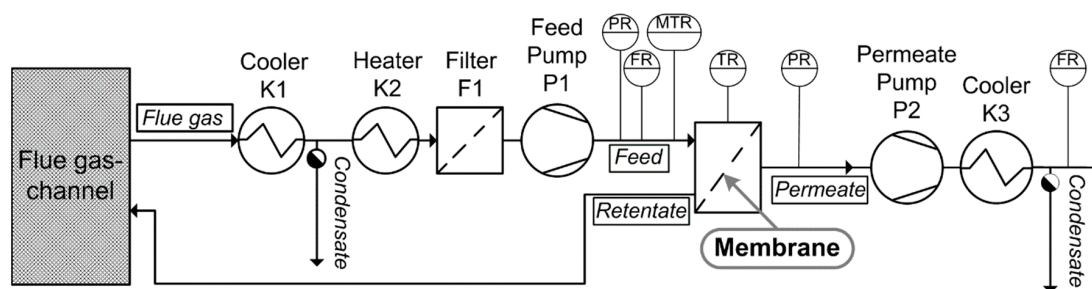


Figure 5. Simplified flow sheet of the single membrane test rig.

2.7.2. Gas Permeation Pilot Plant at Hard Coal-fired Power Plant

The SILM stability was also investigated during operation at the hard coal-fired Rheinhafen-Dampfkraftwerk by EnBW AG in Karlsruhe, Germany. The SILM module was therefore installed in a gas permeation pilot plant (see Figure 6). The pilot plant, which can be run in one-stage parallel mode and in two-stage mode, was previously described by Pohlmann et al. [34]. In contrast to the aforementioned study, the arrangement of the side channel blower (C1) was reconfigured so that the membrane module M1.1 was on the suction side of the blower. This reconfiguration was to prevent the deposition of particulate matter and acidic condensates within the blower housing.

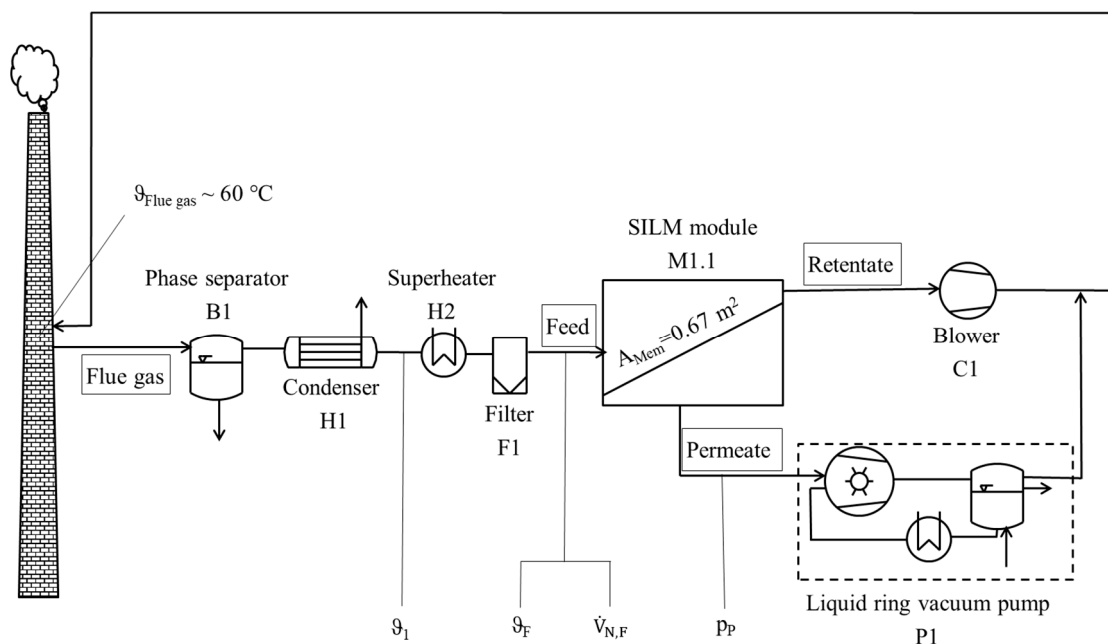


Figure 6. Simplified flow sheet of gas permeation pilot plant.

In order to avoid flue gas condensation within the pilot plant—more specifically, within the module housing—the pilot plant was purged with ambient air for at least one hour before and after flue gas operation. During flue gas operation, a small fraction of the power plant off-gas was sucked out of the power plant chimney into the pilot plant. To avoid membrane damage by acidic condensates during operation, the flue gas was permanently cooled in the condenser H1 to $\vartheta_1 \sim 22$ °C and constantly superheated in the electrical heater H2. The superheating resulted in a nearly constant feed temperature of $\vartheta_F \sim 33$ °C throughout the entire measurement campaign. The feed standard volume flow $\dot{V}_{N,F}$, which is regulated by the rotational speed of C1, was also kept constant ($\dot{V}_{N,F} \sim 5.5$ m³(STP)/h). For a sufficient driving force, the permeate pressure p_p , which is regulated by a pressure control valve, was continuously adjusted to 125 mbar.

2.8. Process Simulation

Steady-state process simulations were run for an indication of the SILM stability during operation at the hard coal-fired power plant. For this purpose, the equation-oriented simulation software Aspen Custom Modeler[®] [35] was used. In-house developed models for the phase separator, heat exchanger, pumps and membrane modules were used to simulate the gas permeation process.

The simulation model of the membrane module was described in detail by Brinkmann et al. [31]. Geometrical parameters were adjusted according to the dimension of the K100 module. Real gas behaviour, concentration polarization and non-isothermal behaviour were considered, as well as the pressure drop in the feed/retentate and permeate channel. An adjustment to the permeate-side pressure drop equation was necessary to achieve a better match between the simulation and

experimental results. For the calculation of gas properties, the cubic Soave–Redlich–Kwong equation of state extended for the better treatment of water vapor according to Kabadi and Danner (SRKKD) [36] as implemented in Aspen Properties used. The permeance L of component i at temperature T was calculated using the model of a membrane module according to the Arrhenius equation:

$$L_i = L_{\text{fac}} \cdot L_{\infty,i}^0 \cdot \exp\left(-\frac{E_i}{R \cdot T}\right), \quad (4)$$

where R is the universal gas constant. The activation energy E_i and the permeance of component i at infinitely high temperature $L_{\infty,i}^0$ were determined using the results of the single gas membrane performance test of the corresponding membrane. The scaling factor L_{fac} was calculated in order to adjust the permeance calculations. This is necessary if differences in the gas permeances of the initial measured SILM stamp (measured with the pressure increase method) and the final SILM module (module quality control results) are found.

For every steady-state run of the process simulation, the measured values of feed temperature ϑ_F , feed standard volume flow $\dot{V}_{N,F}$, feed pressure p_F , feed mole fraction $x_{F,i}$ ($i = \text{CO}_2, \text{N}_2, \text{O}_2$ and H_2O) and permeate pressure p_P were set as fixed variables. Trace substances like SO_x and NO_x , as well as solid and liquid particles (aerosols), were neglected.

3. Results and Discussion

3.1. Investigation of PAN Supports and Coating Solution Influence on SILM Quality

The main aim of the conducted study was to investigate the stability of an SILM during real flue gas operation. To get a mechanically stable SILM that also has in addition a good membrane separation performance, twelve membranes (M1a15/20–M1c15/20 and M2a15/20–M2c15/20) were prepared. The most promising membrane in terms of separation performance was chosen for large-scale SILM production and stability investigation with real power plant flue gas. In this section, the results of the PAN support investigation and SILM separation performance investigation are presented and discussed.

3.1.1. PAN Support Investigation

The stability of an SILM is highly dependent on the morphology of the support membrane. It is assumed that the presence of macro-voids in the support leads to unwanted imperfections in the IL layer and can also result in mechanical damage to the membrane during its use. As can be seen in Figure 1, the six PAN membranes did not have any macro-voids.

Water permeance measurements were taken to determine the regularity of the support membrane morphology. The M1c membrane had the smallest standard deviation for water permeance (see Figure 7); this could be an indication that the M1c support had the most regular morphology over the membrane length. A support membrane with a regular morphology throughout the whole batch is a promising candidate for the preparation of a highly selective, mechanically stable SILM membrane, because imperfections in the IL layer are not likely to occur during selective layer formation.

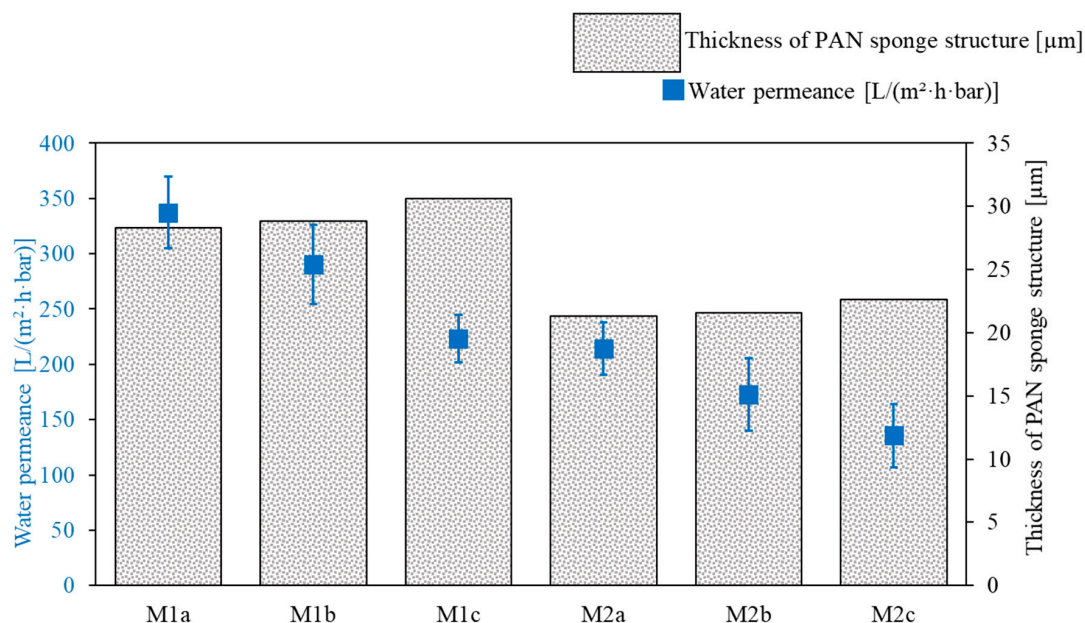


Figure 7. Water permeance and thickness of the PAN membranes M1a–M1c and M2a–M2c used as supports for SILMs.

Comparing the membranes made with the same solvent composition (M1 or M2), it can be seen that the water permeance decreased with increasing PAN membrane thickness. Since all membranes were made with the same amount of PAN (13.4 wt. %) and the M2 membranes were thinner than M1, the M1 supports had a higher overall porosity compared with M2. This was also confirmed by the fact that the water permeances of the M1c and M2a membranes were similar, although M1c had a greater thickness than M2a. The overall porosity of the support substructure can influence the membrane performance of the resulting SILM in several ways. On the one hand, a dense matrix-structure can prevent the IL from penetrating the support too deeply during coating. This would result in a thinner IL layer and, therefore, a higher permeance of the SILM. On the other hand, comparing two SILMs with the same IL thickness, a dense substructure and/or high tortuosity of the support will decrease the membrane permeance, since the permeation distance for the gases (effective selective layer thickness) is higher.

Supported liquid membranes prepared using porous membranes with narrow surface pore size distributions are less sensitive to pressure fluctuations [37]. Furthermore, when using a support with a narrow surface pore size distribution, it is likely that the prepared SILM will have fewer imperfections in the IL layer. From the SEM images (Figure 1), it can be seen that the surfaces of the PAN membranes M1a–M1c and M2a–M2c are similar in morphology. The pores were counted and there were approximately one thousand pores per square micrometre, with a pore diameter of 6 ± 1.86 nm. In terms of surface porosity, isoporous membranes made from PS-*b*-P4VP seem to be better suited for SILM production [18]. Nevertheless, PAN membranes were chosen for SILM production, since PAN membranes can be produced at a large scale, are chemically and mechanically stable for the application at hand, and, therefore, are suitable for scalable membrane preparation.

3.1.2. SILM Investigation

The support membranes M1a–M1c and M2a–M2c, discussed in the previous section, were each coated with two different coating solutions (15 wt. % and 20 wt. % IL in methanol). The twelve resulting SILMs were then subjected to single gas measurements. In this section, the dependence of the resulting selectivities and permeances on the support properties and coating solution properties is briefly discussed.

First, the single gas measurement results showed that using a coating solution with a lower IL concentration resulted in more permeable SILMs (Figure 8). It is probable that a higher concentration of IL in the coating solution leads to a greater pore volume over the membrane thickness being filled with the IL, what in turn results in lower permeances.

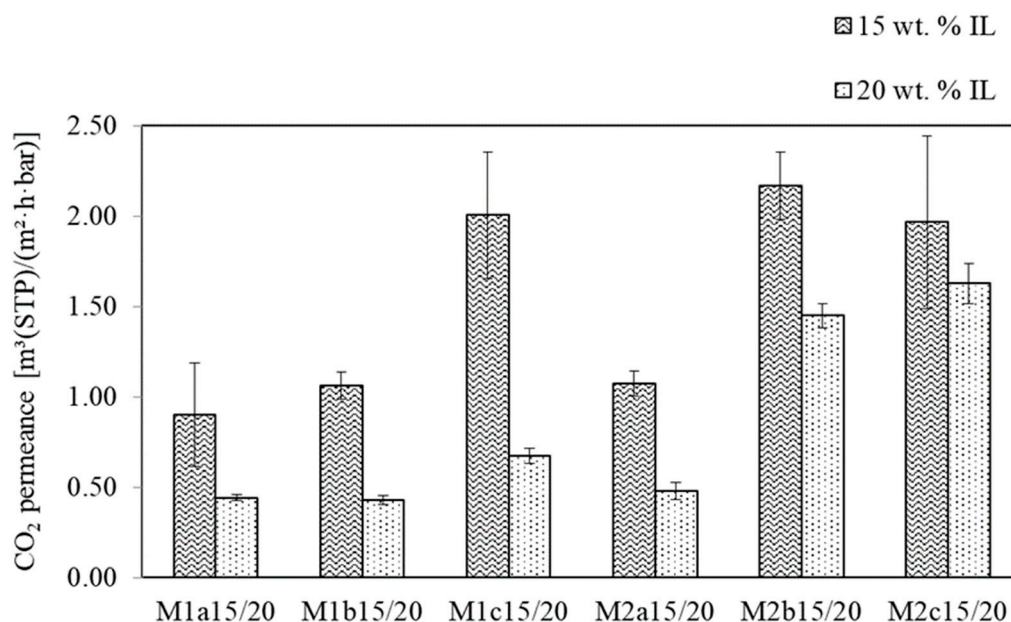


Figure 8. CO₂ single gas permeances of M1/2a15/20–M1/2c15/20 at $\vartheta = 28\text{ }^{\circ}\text{C}$ and $\Delta p = 2\text{ bar}$.

Secondly, comparing the membranes M1 and M2, it can be seen that the coating solution composition had different effects on the selectivity. The M1 membranes were more selective when coated with the 15 wt.% coating solution. The opposite was found for the M2 membranes, for which the 20 wt.% coating solution led to more selective SILMs (Figure 9).

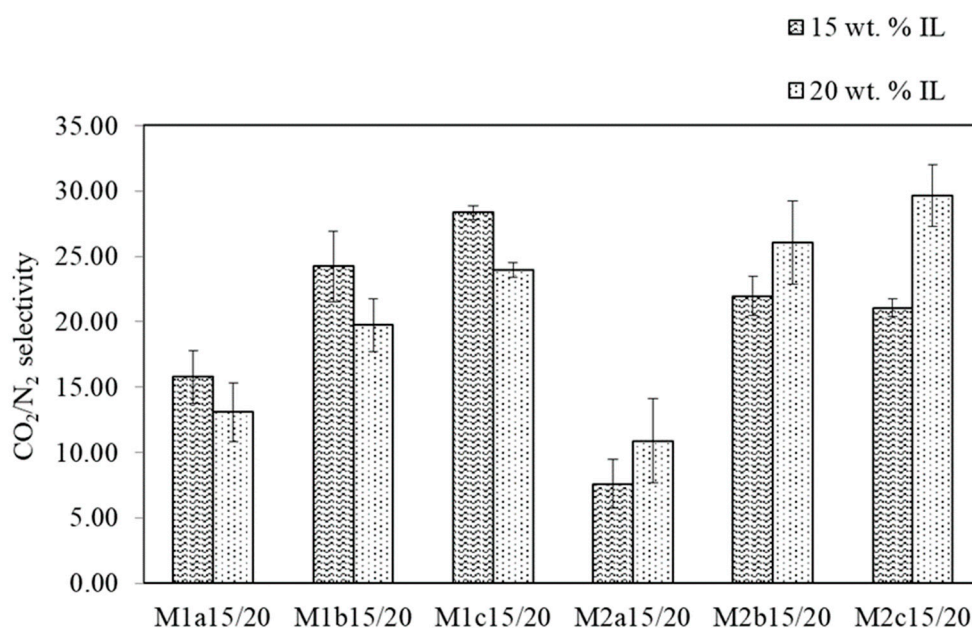


Figure 9. CO₂ single gas selectivities of M1/2a15/20–M1/2c15/20 ($\vartheta = 28\text{ }^{\circ}\text{C}$, $\Delta p = 2\text{ bar}$).

A conclusive explanation or prediction for the above observation and for the dependence of the selectivities and permeances on the overall porosity of the support membranes was not found. This

is likely due to the fact that the properties of the porous support, as well as the properties of the coating solutions, can influence the SILM performance in positive and/or negative ways. This was briefly discussed regarding the influence of the overall support membrane porosity on the resulting permeance of the SILMs (see Section 3.1.1). There is another proposed mechanism that could explain the varying effects of IL concentration in the coating solution. On the one hand, due to the lower viscosity, less concentrated coating solutions are likely to more deeply penetrate the pores of a support. On the other hand, this does not automatically result in a lower permeance: since the amount of IL is lower, it therefore fills less pore volume.

Our primary aim for this study was to investigate the SILM stability during real flue gas operation. We decided to prepare M1c15 on a large scale, because this variant showed the best overall membrane performance.

3.2. SILM Large-Scale Preparation and Quality Control: From SILM Sheet to SILM Module

Prior to the stability investigations of SILMs operating in power plant flue gas, the M1c15 membrane was prepared on a pilot scale. An SILM sheet having a membrane area of about six square meters was prepared. From that batch, 59 intact membrane envelopes were prepared and incorporated into a membrane module having a total membrane area of 0.67 m². In this section, the results of the pressure increase measurements, as well as the results of quality control testing after each step of preparation (from membrane sheet to module), are presented and discussed.

3.2.1. “Pressure Increase” Measurements

Figure 10 shows the temperature depending permeances of CO₂, O₂ and N₂ of the pilot scale produced M1c15 SILM in the form of an Arrhenius plot. The data were determined with the “pressure increase” (constant volume/variable pressure) method. A temperature range of 21–67 °C was chosen for the investigation, because this is a typical range for the feed temperature during flue gas operation ($\vartheta_F \sim 33\text{--}40$ °C). As can be seen, within the investigated temperature range, the permeance of the measured components increased with increasing temperature. However, no conclusions about the dependence of permeance on temperatures outside of the investigated range should be drawn from these results, since this trend can change at other temperatures. This is due to the fact that the permeation of a gas is mostly influenced by sorption to and diffusion through the ionic liquid and the two processes exhibit opposing temperature dependencies. Furthermore, the permeability can also be influenced by material flow through open pores, since imperfections in the IL layer are likely to be present in the SILM M1c15.

The mean pressure between feed and permeate during the pressure increase measurements was chosen to be about 250 mbar for all gases. One has to keep in mind that, during real flue gas operation, the mean pressure is different for each component since the mole fraction of each component is different in the feed stream, as well as in the permeate stream. In addition, the total mean pressure slightly fluctuates during operation, although p_F and p_P were adjusted to a constant value. The dependence of the permeances on the mean pressure was not investigated in detail and hence neglected in process simulation. The temperature-dependent permeance was calculated in the simulation model according to the Arrhenius equation (Equation (4)). The Arrhenius model parameters (Table 3) were determined from the pressure increase results.

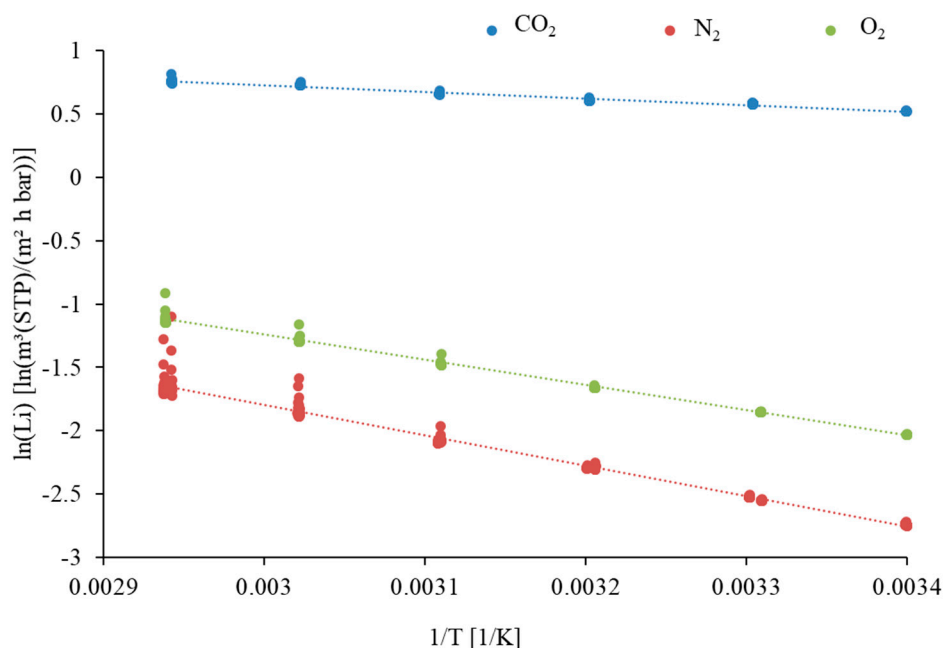


Figure 10. Arrhenius plot of the temperature depending single gas permeances of CO₂, N₂ and O₂ of SILM M1c15 (average pressure ~250 mbar).

Table 3. Arrhenius model parameters of CO₂, O₂ and N₂ (temperature range of 21–67 °C).

Component	L _i at 33 °C [m ³ (STP)/(m ² ·h·bar)]	L _{∞,i} ⁰ [m ³ (STP)/(m ² ·h·bar)]	E _i [kJ/mol]
CO ₂	1.82	6.21	3.122
O ₂	0.17	74.00	15.439
N ₂	0.09	206.00	19.766

The results of the pressure increase measurements showed that the previous selectivity and permeance values (i.e., the measurements attained during the PAN support and IL-coating investigation campaign for SILM M1c15 ($\alpha_{\text{CO}_2/\text{N}_2} = 28.35 \pm 0.51$ and $L_{\text{CO}_2} = 2.00 \pm 0.35$ m³(STP)/(m²·h·bar); Figures 8 and 9)) could not be achieved again after the large-scale preparation of M1c15. This reveals issues concerning the reproducibility of a qualitatively equal SILM. Nevertheless, the results show that it is possible to prepare an SILM on a large scale with a pilot-scale coating machine and a porous PAN support.

3.2.2. SILM Envelope and Module Preparation

SILM envelopes were prepared from the M1c15 large-scale batch and quality control testing of these envelopes was carried out using single gas measurements. Then, satisfactorily performing envelopes were selected and packed into a K100 module housing. Lastly, quality control testing of the SILM module was performed with single gases and compressed air.

In total, 79 membrane envelopes were welded. Of this group, 59 intact envelopes were chosen for module preparation. In Table 4, the average results of single gas SILM envelope quality control measurements are reported.

Table 4. Average CO₂ permeance, CO₂/N₂ selectivity and O₂/N₂ selectivity of SILM envelopes ($\vartheta = 20\text{ }^{\circ}\text{C}$, $\Delta p = 2\text{ bar}$).

Total Membrane Area [m ²]	L _{CO₂} [m ³ (STP)/(m ² ·h·bar)]	$\alpha_{\text{CO}_2/\text{N}_2}$ [-]	$\alpha_{\text{O}_2/\text{N}_2}$ [-]
0.67	1.53 ± 0.35	22.97 ± 1.54	1.79 ± 0.34

The main factor driving envelope selection was CO₂/N₂ selectivity because it enables a clear observation of CO₂ enrichment of the permeate during flue gas operation; this, in turn, gives a strong indication of membrane stability. An average CO₂ permeance of 1.53 m³(STP)/(m²·h·bar) at 20 °C was assumed to be sufficiently high. The average CO₂ permeance of the envelopes revealed that the large-scale SILM batch had irregularities in IL thickness, since a standard deviation of 0.35 m³(STP)/(m²·h·bar) was determined and a permeance of 1.72 m³(STP)/(m²·h·bar) at 20 °C was calculated using the Arrhenius parameters (Table 3).

After preparation of the SILM module, the permeances of O₂ and N₂ were determined with both compressed air and single gases at $\vartheta = 25\text{ }^{\circ}\text{C}$ and $\Delta p = 2\text{ bar}$ (Table 5) for quality control. Testing with CO₂ was not possible since the CO₂ permeate volume flow was out of the measuring range of our Bios Defender 220 flow meter.

Table 5. Results of SILM module quality control with compressed air and single gases ($\vartheta = 25\text{ }^{\circ}\text{C}$, $\Delta p = 2\text{ bar}$).

Feed Gas for Quality Control	L _{O₂} [m ³ (STP)/(m ² ·h·bar)]	L _{N₂} [m ³ (STP)/(m ² ·h·bar)]	$\alpha_{\text{O}_2/\text{N}_2}$ [-]
Compressed air	0.12	0.09	1.33
Single gases	0.13	0.08	1.63

Comparing the results of SILM module quality control and SILM envelope quality control, it can be seen that the module preparation did not introduce any leakages to the module. Differences in O₂/N₂ selectivities, when using compressed air or single gases, can be simply explained by the sensitivity of the selectivity calculation, since small inaccuracies during measurements cause large deviations in selectivity calculations.

For the process simulation, the factor $L_{\text{fac}} = 0.81$ was calculated by dividing the N₂ permeance calculated with the Arrhenius equation at 25 °C and the N₂ permeance determined with the compressed air module quality control results. The scaling factor (see Equation (4)) was then included in the simulation model as a fixed variable.

3.3. SILM Stability Investigation during Flue Gas Operation

In this section, the results of the SILM stability investigation during real power plant flue gas operation are presented. The separation properties of the membrane before and after flue gas operation are reported and discussed. Differences in flue gas compositions at both experimental sites are described and related to the SILM stability investigation results.

3.3.1. Gas Permeation Test Stand Investigation at Lignite-Fired Power Plant

Two experiments with samples of the SILM M1c15 material were carried out at the power plant in Niederaussem. Figure 11a shows a membrane sample before exposure; Figure 11b shows sample 1 after 113 h of operation; and Figure 11c shows sample 2 after 335 h of flue gas operation. The membrane area of the samples is 8 cm². When removing sample 1 (Figure 11b), parts of the membrane became stuck to the test cell sealing ring; apart from this, there were no visible changes in the samples caused by flue gas exposure.

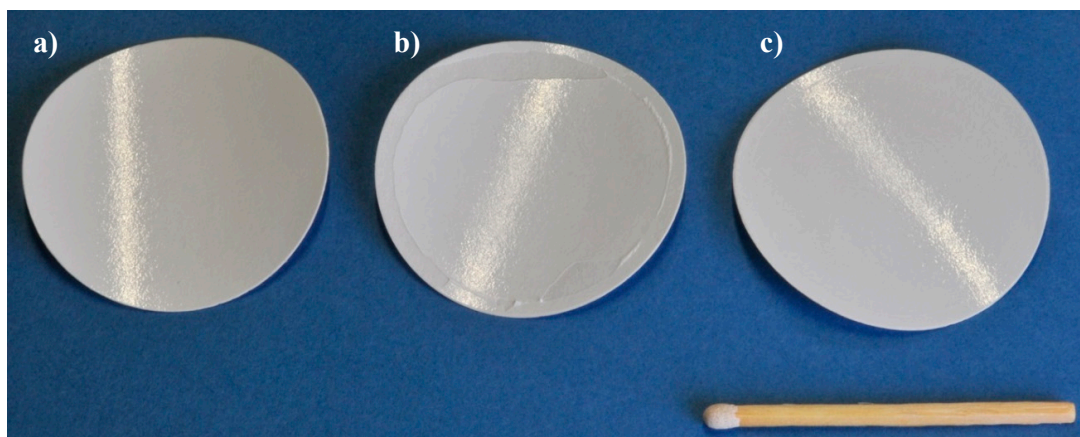


Figure 11. Samples used for the two experiments; (a) new sample; (b) sample 1 after exposure for 113 h; (c) sample 2 after exposure for 335 h.

The data from the experiment with sample 1 are shown in Figure 12. The test lasted for 113 h and the experiment was performed under flue gas conditions for the first 70 h (before the FGDplus system ceased operation).

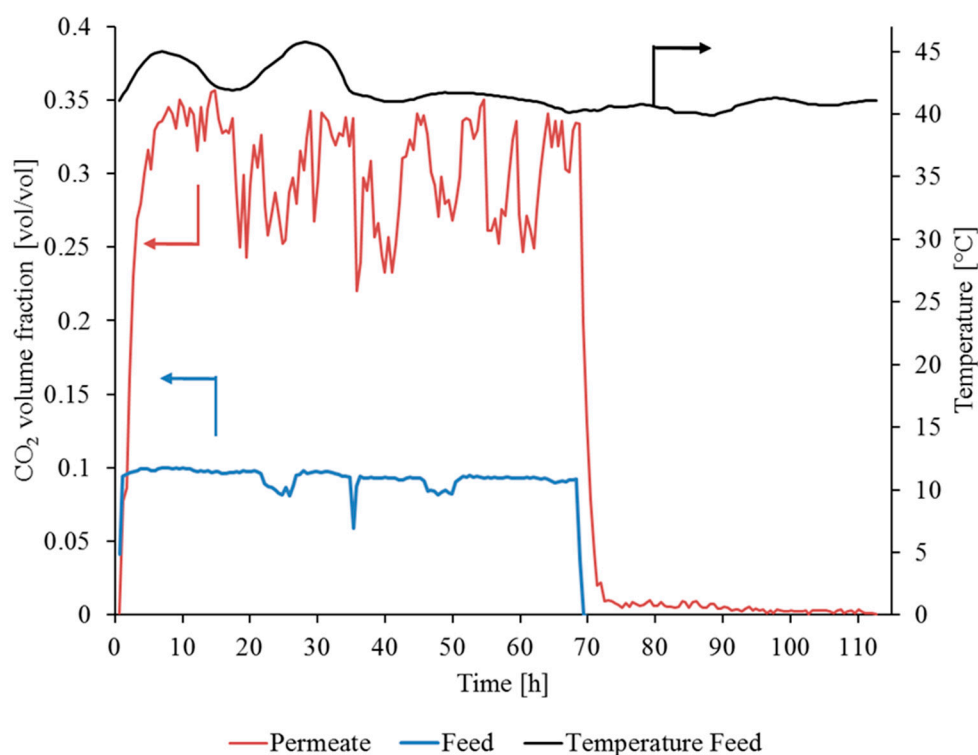


Figure 12. Operation of SILM sample 1 in flue gas: $y_{F,CO_2}, \vartheta_F, \dot{V}_{N,F} \sim 0.12 \text{ m}^3(\text{STP})/\text{h}, p_p \sim 20 \text{ mbar}$.

The measurement data from the test stand in the power plant did not indicate deterioration in the membrane performance during flue gas operation (see Figures 12 and 13). The fluctuations in CO₂ concentration in the permeate (red line) are the result of the low permeate flow causing unstable measured values. This observation is, however, not critical to the qualitative assessment of the SILM stability. The constant increase in CO₂ concentration from a volume fraction of 0.09 (Feed) up to a volume fraction of 0.35 (Permeate) for the first 70 h proves the stability of the membrane under flue gas conditions.

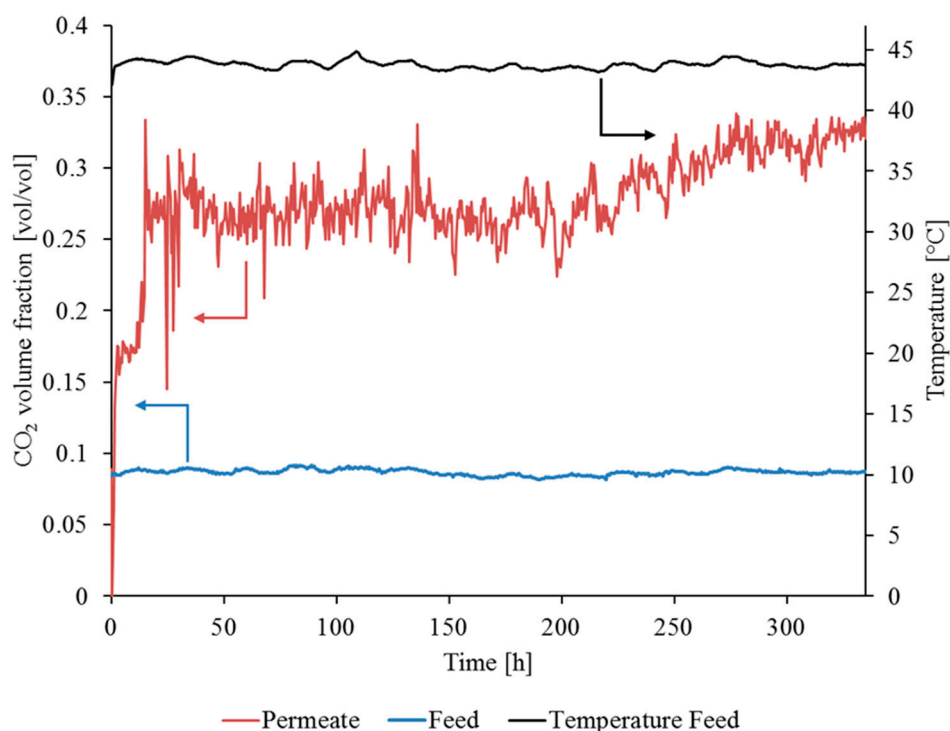


Figure 13. Stable operation of SILM sample 2 in flue gas: y_{F,CO_2} , y_{P,CO_2} , ϑ_F , $\dot{V}_{N,F} \sim 0.12 \text{ m}^3(\text{STP})/\text{h}$, $p_p \sim 20 \text{ mbar}$.

The second test was carried out with a new membrane stamp (sample 2) for 335 h with a continuous supply of flue gas (Figure 13). Again, there was considerable fluctuation in the CO_2 permeate concentration caused by the permeate flow being too low. By comparing tests 1 and 2, the lower concentration of CO_2 in the permeate (an average volume fraction of 0.28) can be explained by the lower CO_2/N_2 selectivity of sample 2 (see Table 6). An explanation for the slight increase in the CO_2 concentration in the permeate during the measurement campaign is rather speculative and could be due to the membrane or measurement inaccuracy. Overall, the results show no degradation in membrane performance during the flue gas operation under the test conditions.

Table 6. Single gas measurements of M1c15 sample 1 and sample 2 performed before and after the experiment in the flue gas ($\vartheta = 35 \text{ }^\circ\text{C}$, $\Delta p = 3 \text{ bar}$).

Parameter	Sample 1		Sample 2	
	Before Experiment	After Experiment	Before Experiment	After Experiment
CO_2 permeance [$\text{m}^3(\text{STP})/(\text{m}^2 \cdot \text{h} \cdot \text{bar})$]	2.43	2.68	2.46	2.90
N_2 Permeance [$\text{m}^3(\text{STP})/(\text{m}^2 \cdot \text{h} \cdot \text{bar})$]	0.09	0.16	0.11	0.45
CO_2/N_2 selectivity [-]	27.00	17.11	22.36	6.44

Aiming to derive a quantitative expression of the membrane performance before and after the flue gas exposure, single gas permeation tests were performed on the two samples. The results are summarized in Table 6 and show significant differences in single gas selectivity and permeance before and after contact with the flue gas. These disparities contradict the results obtained from the test stand experiments and can only be explained by the changes occurring after the end of the flue gas exposure. The changes in the membrane permeances and selectivities observed after flue gas exposure may be due to a loss of IL from the matrix-structure since the selectivity decreased and the CO_2 and N_2 permeances increased.

3.3.2. Gas Permeation Pilot Plant Investigation at Hard Coal-Fired Power Plant

To investigate the SILM stability, the SILM module was installed in the gas permeation pilot plant (Figure 6), which is located at the EnBW hard coal-fired power plant in Karlsruhe, Germany.

Figure 14 shows the CO₂ volume fraction in the feed and permeate, as well as the feed temperature, measured during the first flue gas operation period. The percentage of CO₂ increased from approx. 14 vol. % in the feed to an average value of 35 vol. % in the permeate. It can be observed that the SILM performed stably during the first flue gas operation period. This can be concluded because, considering the trend for y_{F,CO_2} , and ϑ_F , the trend for y_{P,CO_2} is reasonable. During the first 9 h of flue gas operation, the volume fraction of CO₂ in the permeate decreased due to the decreasing CO₂ volume fraction in the feed and the increasing feed temperature. After approx. 14 h, the volume fraction in the feed increased, which, in turn, resulted in an increasing CO₂ volume fraction in the permeate. A further indication of the stable performance of the SILM module during the first operation period is the good match between the experimental and simulation results of y_{P,CO_2} .

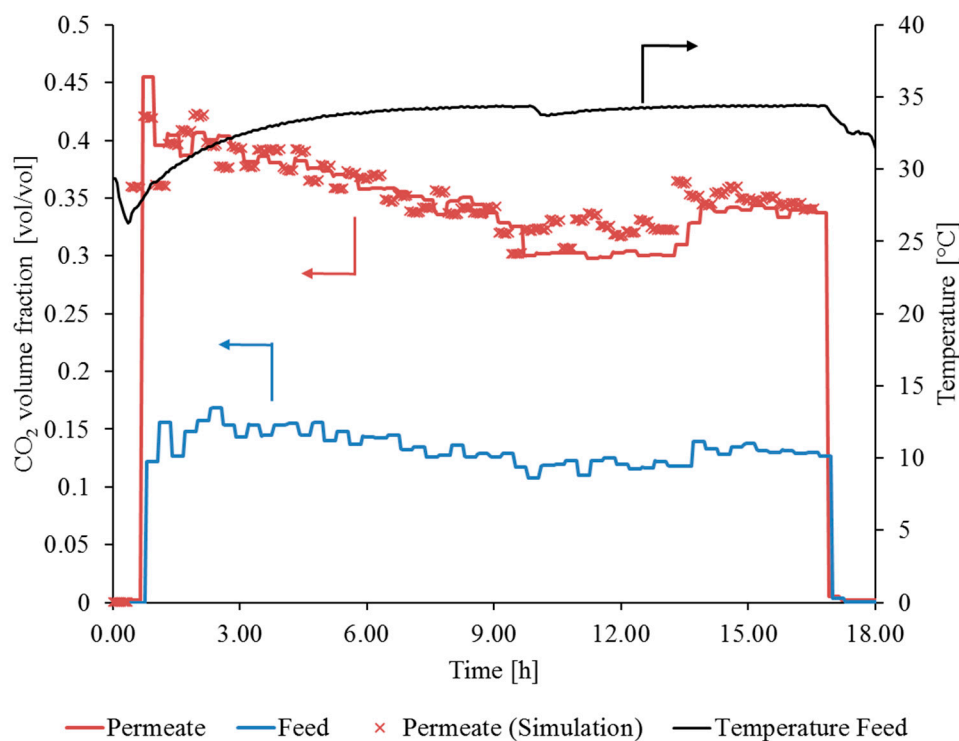


Figure 14. Stable operation of SILM in flue gas: y_{F,CO_2} , y_{P,CO_2} , ϑ_F during first flue gas operation period, $\dot{V}_{N,F} \sim 5.5 \text{ m}^3(\text{STP})/\text{h}$, $p_p \sim 125 \text{ mbar}$.

After approx. 17 h of flue gas operation, the investigation had to be stopped due to power plant downtime, which lasted for 17 days. After 432 h, the SILM module stability investigation resumed.

From the beginning of the second flue gas operation period, the volume fraction of CO₂ in the permeate constantly decreased until $t = 462 \text{ h}$, at which time a nearly constant CO₂ volume fraction in the permeate was observed. The gap between experimental and simulation results increased, illustrating that the SILM module was damaged during the second flue gas operation period at the hard coal-fired power plant in Karlsruhe. Issues regarding feed concentration measurements from $t = 432 \text{ h}$ to $t = 442 \text{ h}$ have to be mentioned, since such high values for y_{F,CO_2} (up to 0.2 vol/vol) are not realistic in the flue gas of coal-fired power plants (see Figure 15). This also explains why the experimental and simulation results do match well at the beginning of the second flue gas operation period.

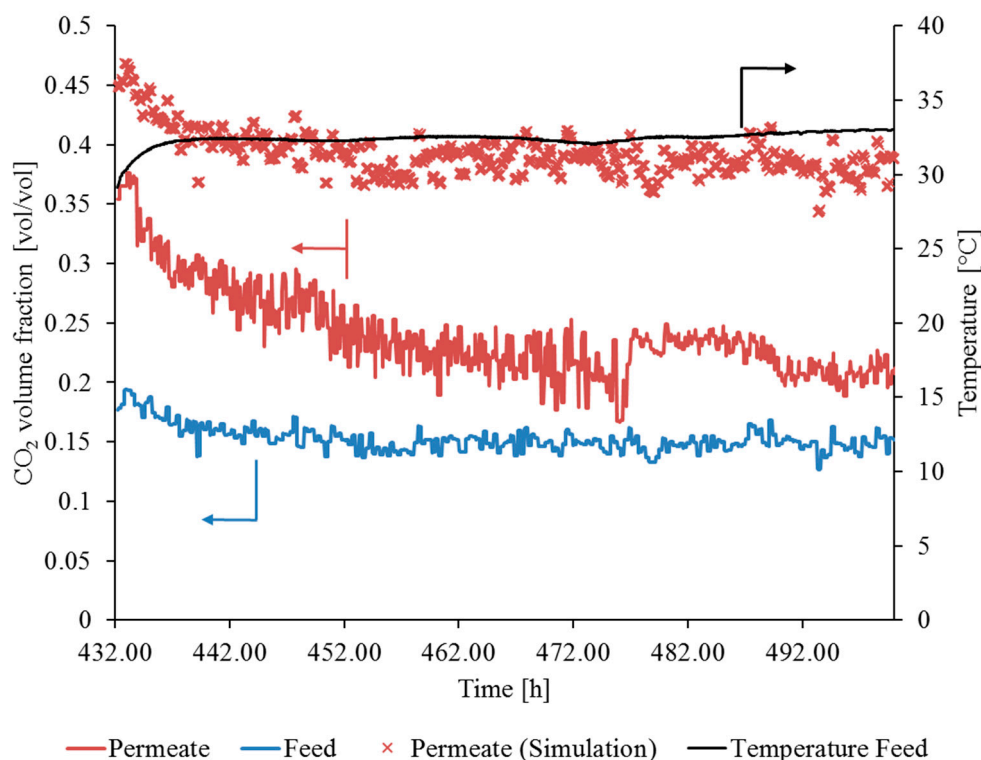


Figure 15. SILM failure during flue gas operation: y_{F,CO_2} , y_{P,CO_2} , ϑ_F during second flue gas operation period, $\dot{V}_{N,F} \sim 5.5 \text{ m}^3(\text{STP})/\text{h}$, $p_p \sim 125 \text{ mbar}$.

After the measurement campaign, the SILM module was removed from the pilot plant and follow-up examinations were performed to investigate possible causes of membrane damage. The SILM envelopes were removed from the module housing and the average relative change in single gas permeances after flue gas operation was determined (Table 7).

Table 7. Results of SILM envelope test before and after flue gas operation ($\vartheta = 20 \text{ }^\circ\text{C}$, $\Delta p = 2 \text{ bar}$).

Component	CO ₂	O ₂	N ₂
Average permeance before flue gas operation [m ³ (STP)/(m ² ·h·bar)]	1.53 ± 0.35	0.12 ± 0.03	0.07 ± 0.02
Average relative change of permeance after flue gas operation [%]	−41 ± 8	41 ± 40	131 ± 84

Unlike the SILM samples measured at the lignite-fired power plant, these samples did not show a loss of IL after flue gas exposure. This is because the average CO₂ permeance was lower, whereas the average permeances of O₂ and N₂ were higher after flue gas operation. This agrees with an average CO₂/N₂ selectivity of 6.6 ± 3.5 and an average O₂/N₂ selectivity of 1.1 ± 0.1 .

In order to avoid membrane damage, on the one hand, the pilot plant was always purged for one hour with ambient air before and after flue gas operation. On the other hand, a drop in flue gas temperature to below its dew point temperature in the membrane module was prevented by the pilot plant’s pre-treatment steps (see Figure 6). The flue gas was cooled down in H1 and subsequently superheated in H2 before entering the membrane modules M1.1 and M1.2 (in one-stage parallel mode). Hence, the membrane damage due to the deposition of acidic condensates on the membrane surface can be excluded. To draw conclusions about the cause of membrane damage during flue gas operation in Karlsruhe, the differences in the power plants’ off-gas composition at both experimental sites were compared.

3.4. Comparison of Flue Gas Compositions at Both Experimental Sites

The SILM performed stably during flue gas operation for at least 335 h at the power plant in Niederaussem, whereas the membrane was quickly damaged during operation at the power plant in Karlsruhe. The composition of a power plant's off-gas is influenced by the fuel, combustion conditions and flue gas cleaning steps. In this section, the differences in coal and flue gas cleaning at both power plants are reported and discussed. The results uncover the reason for the nearly immediate damage of the SILMs when operating at the power plant in Karlsruhe.

First of all, it has to be mentioned that the RWE power plant in Niederaussem is lignite-fired, whereas the EnBW power plant in Karlsruhe is hard coal-fired. Usually, lignite has a higher sulphur content compared with hard coal; consequentially, the concentration of SO_x in the flue gas of lignite-fired power plants is higher than that in hard coal-fired power plants when comparing non-cleaned flue gas streams. The Rhenish lignite has a relatively low concentration of sulphur compared with lignite from other sources, so conclusions about the differences in SO_x concentrations in both flue gases due to the coal types would be vague. In addition, the quality of the coal at both power plants slightly changes from time to time, so a conclusion about membrane damage due to coal quality is hardly possible.

The composition of the power plant off-gases is influenced by the different flue gas cleaning steps. Both power plants are equipped with standard cleaning steps for particulate removal (dry electrostatic precipitator (ESP)) and removal of sulphur oxides (wet flue gas desulfurization (WFGD)). The WFGD is used in general at both power plants; however, at RWE Niederaussem, a high-performance FGD pilot plant [33] (FGDplus pilot plant from ANDRITZ Energy & Environment) is under investigation and was in operation during the SILM measurement campaign upstream of the gas permeation test stand. The FGDplus pilot plant is constructed modularly and consists of a total of five modules (counter flow module, FGDplus module, spray tower module, droplet separator module and wet electrostatic precipitator module (WESP)) [38]. The concentration of SO_x in the power plant off-gas is further reduced by the FGDplus pilot plant compared with the generally used WFGD. Nevertheless, this does not seem to be the key difference between the two power plants, which is decisive for stable membrane performance. The main difference in general flue gas cleaning between the RWE power plant (block K) in Niederaussem and the EnBW power plant (block 8) in Karlsruhe rather lies in the way that nitrogen oxides are avoided/reduced. At the RWE power plant in Niederaussem, the concentration of NO_x is held under its legal limit by using combustion measures, whereas a selective catalytic reduction (SCR) with ammonia as the reducing agent is used in Karlsruhe.

Our research led us to a problem that was observed for post-combustion amine absorption processes [38–40]—the presence of solid and liquid aerosols in power plant flue gases. Liquid SO_3 aerosols are known to form in the flue gas of sulphur-containing fuels. The formation of small sulfuric acid droplets with a diameter $\leq 10 \mu\text{m}$, also termed mist or fog, was previously described by Schaber (1995) [41]. Water vapor and SO_3 in the flue gas react to form gaseous H_2SO_4 . In addition, we know from Li et al. [42] that the ammonia (NH_3) used in an SCR can react with H_2O and SO_3 to generate ammonium sulphate ($(\text{NH}_4)_2\text{SO}_4$) and/or bisulphate (NH_4HSO_4). The rapid drop in temperature in the WFGD leads to the supersaturation of all SO_3 molecules and homogeneous liquid and/or heterogeneous solid–liquid aerosols are formed by nucleation mechanisms [43]. Most of the SO_3 molecules (H_2SO_4 , $(\text{NH}_4)_2\text{SO}_4$, NH_4HSO_4) stay in the gaseous state until they reach the WFGD. In cooler regions of the flue gas flow path, condensation of the SO_3 molecules can even occur before entering the WFGD. Comparing the flue gas cleaning steps of both power plants and their influence on aerosol formation results in a reasonable explanation for the membrane damage in Karlsruhe compared with the stable SILM operation in Niederaussem (see Table 8)—the presence of larger quantities of SO_3 aerosols, such as sulfuric acid and especially sticky ammonium sulphate and/or bisulphate, in the EnBW power plant (block 8) in Karlsruhe. In particular, the formation of sticky ammonium sulphate and bisulphate aerosols due to the presence of ammonia as a reducing agent in an SCR [42] is possible at the EnBW power plant in Karlsruhe. In addition, it is likely that more gaseous H_2SO_4 formed in

Karlsruhe since the additional oxidation of SO₂ to SO₃ may occur in an SCR [42]. Additional SO₃ may have also formed in the ESP [38], which applies to both power plants. Another factor for aerosol formation, which was not proven by us, may be the temperature difference during the desulfurization step, since the homogeneous (liquid) and heterogeneous (solid–liquid) SO₃ aerosols form in the WFGD. A smoother cooling of the flue gas within the WFGD probably results in fewer SO₃ aerosols being formed. The flue gas at the RWE power plant cools from 105 °C to 67 °C [38], whereas the flue gas at the EnBW power plant undergoes sharper cooling, from 140 °C to 65 °C (see Table 8).

Table 8. Comparison of coal type and flue gas cleaning steps of both power plants and the influence on formation of SO₃ aerosols.

Power Station	Coal Type	SCR	ESP	FGD
RWE Niederaussem (block K)	Rhenish low-sulphur lignite	NO (reduction of NO _x by combustion measures)	YES	WFGD and FGDplus pilot plant ($\Delta T = 105\text{--}67\text{ }^\circ\text{C}$ [38])
EnBW Karlsruhe (block 8)	Different hard coals	YES	YES	WFGD ($\Delta T = 140\text{--}65\text{ }^\circ\text{C}$)
Influence on formation of SO ₃ aerosols	- the higher the content of sulphur, the higher the percentage of SO ₂ and thus SO ₃ in the flue gas	- catalytic enhancement of SO ₂ oxidation to sulphur trioxide (SO ₃) [42] - due to the reducing agent, ammonia (NH ₃), ammonium sulphate and/or bisulphate may be formed [42]	- the oxidation of SO ₂ to SO ₃ could occur as a result of ozone formation [38]	- sharp cooling of the flue gas in the FGD causes aerosol formation by heterogeneous or homogeneous nucleation due to supersaturation [43]

Another argument for small-size droplets (nanometre scale) being the cause of membrane damage is that aerosols are hardly separated by the pilot plant's pre-treatment steps. During the previous PolyActive™ measurement campaigns [34], where the blower C1 was arranged upstream of the membrane modules M1.1 and M1.2 (in one-stage parallel mode (see Figure 6), membrane damage as described in this publication was not observed. The membrane showed a stable performance but issues with gypsum particles and acidic depositions within the blower housing were observed. It was decided to install the blower C1 downstream of the membrane modules for the current measurement campaign. That, in turn, probably prevented the aerosols from becoming stuck in the blower housing, so they were deposited in the membrane module. Because of the sharp changes in the flow directions and feed spacers within the module housing [31], the especially sticky (NH₄)₂SO₄ and/or NH₄HSO₄ aerosols could have deposited on the membrane surface. Another possible reason for the stable performance of the PolyActive™ module in the previous measurement campaign [34] is that the pilot plant was operating at block 7 at the EnBW power plant during the previous measurement campaign and it is very likely that smaller quantities of aerosols were in the off-gas of block 7. This is because, on the one hand, low-sulphur coal was burned during our measurement campaigns at block 7. On the other hand, the flue gas was reheated before entering the corrodible chimney of block 7.

To underpin the presumption that the SILM damage was caused by SO₃ aerosols, the SILMs that were used in Karlsruhe were analysed for the presence of NH₄⁺ and SO₄²⁻. Therefore, eight stamps ($A_{\text{total}} = 49.3\text{ cm}^2$) of the flue-gas-exposed SILMs and non-flue-gas-exposed SILMs were each washed for one week with 100 mL of ultrapure water at 50 °C. The concentrations of NH₄⁺ were then photometrically determined by the EnBW laboratory staff and the concentrations of SO₄²⁻ were determined by ion chromatography. The results are shown in Table 9.

Table 9. Concentration of NH₄⁺ and SO₄²⁻ in the membrane washing solutions.

SILM	c(SO ₄ ²⁻) [mg/L]	c(NH ₄ ⁺) [mg/L]
Non-flue-gas-exposed	<0.1	0.54
Flue-gas-exposed	<0.1	10.4

Low concentrations of SO_4^{2-} ($c(\text{SO}_4^{2-}) < 0.1 \text{ mg/L}$) in the washing solutions were found. However, the performed tests revealed clearly that a higher amount of ammonium was deposited on the membranes after flue gas exposure. For additional evidence on the accumulation of acidic species on the membrane surface, three of the flue-gas-exposed SILM envelopes (Figure 16) were dried under vacuum for 15 h at $50 \text{ }^\circ\text{C}$ and subsequently wetted with distilled water. The pH value was then determined using litmus paper (Figure 16 (top)). The acidic liquid (pH value = 1–2) was verified to contain SO_4^{2-} on the basis of its white turbidity appearance (formation of barium sulphate (BaSO_4)) upon being mixed with barium chloride solution (BaCl_2). No visible change was observed when being mixed with sodium chloride, ammonium chloride or calcium chloride solution (Figure 16 (bottom)).



Figure 16. Acidic liquid on SILM envelopes (top) proven to contain SO_4^{2-} (white turbidity (BaSO_4) in BaCl_2) (bottom).

The litmus test was repeated with the SILMs that were used in Niederaussem, block K. The applied liquid at the surface had a pH value of 7, just like the results of the same test with non-flue-gas-exposed SILMs. Therefore, the possibility of acidic species accumulating on the surface of the SILMs operating in Niederaussem can be excluded. The final investigation established that SO_3 aerosols are very likely the cause of the SILM damage during flue gas operation at the EnBW power plant (block 8) in Karlsruhe, since SO_4^{2-} and NH_4^+ were proven to be deposited on the membranes.

To summarize, it can be concluded that the presence of aerosols in power plant off-gases not only seems to be an issue for post-combustion absorption processes but is also a general problem for post-combustion carbon capture technologies. Na_2SO_4 aerosol with very small solid particles (characteristic particle size $d_p < 50 \text{ nm}$) appears to be the main cause of amine loss at the amine-based post-combustion absorption pilot plant in Niederaussem but effective countermeasures have been reported [39]. Liquid and sticky SO_3 aerosols also cause amine losses but are especially a problem for post-combustion gas permeation processes when present in large quantities in the power plant off-gas, since the membrane can be blocked or chemically degraded.

4. Conclusions

A method to successfully transfer the production of an SILM from the laboratory to pilot scale is presented in combination with a thorough investigation of the required quality of the employed porous support membrane. As far as we know, this is the largest area of an SILM ($A_{Mem} \sim 6 \text{ m}^2$) to be prepared and subsequently mounted into a test cell and pilot plant membrane module ($A_{Mem} = 0.67 \text{ m}^2$).

The SILM was tested under real-life flue gas conditions at lignite- and hard coal-fired power plants. The volume fraction of carbon dioxide in the flue gas was raised from approx. 14 vol. % (feed) to 40 vol. % (permeate).

The results show that the separation of CO_2 from power plant flue gases by gas permeation using SILMs is worthy of consideration and investigation in the future, since the stability of an SILM persisted for at least 335 h when sticky $(\text{NH}_4)_2\text{SO}_4$ and/or NH_4HSO_4 aerosols were absent and H_2SO_4 aerosols in low quantities in the flue gas. The influence of SO_3 aerosol formation on the power plant cleaning steps is summarized. The presence of SO_3 aerosols is a general problem for CC technologies. When an SCR for the reduction of NO_x is used, special efforts ought to be undertaken, either by removing existing aerosols or by preventing the formation of aerosols.

Nevertheless, keeping the investment costs for the membranes in mind, an SILM lifetime longer than 250 h is to be proven. In addition, to date, the membrane performance of PEO-containing polymer membranes, like PolyActive™ and Polaris™, exceeds that of the SILM used in this study. However, there is potential for high-permeance membrane development [21] when using ILs for gas-separating membranes. Figure 17 shows a CO_2/N_2 selectivity versus CO_2 trade-off plot where the enclosed area represents the region of permeability versus selectivity which is desirable for CO_2 separation from flue gas as suggested by Merkel et al. [44]. Inside this region the pressure ratios, required membrane area and feed side gas velocities needed for good membrane performance are in an economically viable regime.

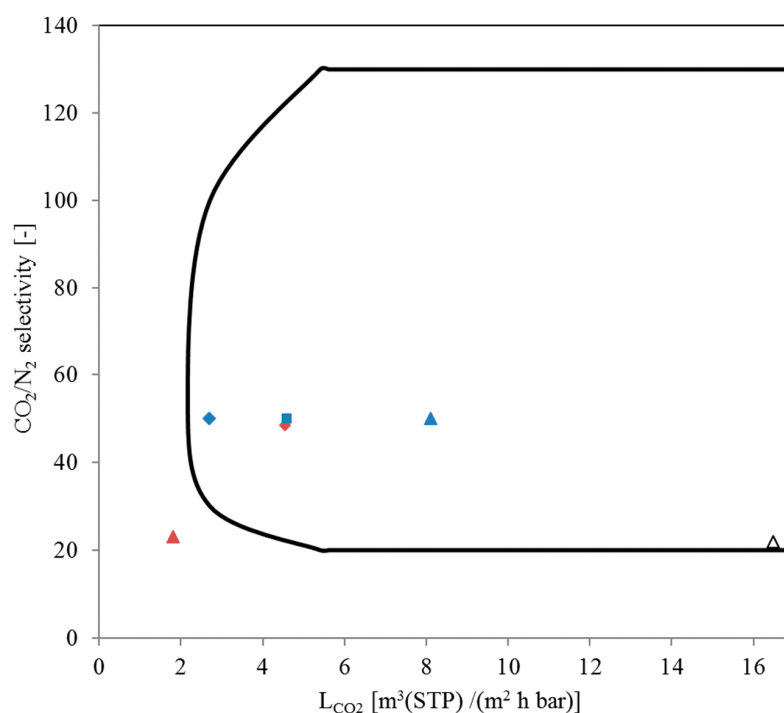


Figure 17. CO_2/N_2 selectivity vs. CO_2 permeance trade-off plot [44]/Comparison of IL membranes with polymeric membranes: \blacklozenge Polaris™ Gen-1 (commercial scale) [11]; \blacksquare Polaris™ Gen-2 (pilot scale) [11]; \blacktriangle Polaris™ advanced (lab scale) [11]; \blacklozenge PolyActive™ 1500 [9]; \blacktriangle SILM with EMIM Tf2N Δ TFCM with EMIM Tf2N [21].

Author Contributions: Conceptualization and project administration, P.K.; SILM preparation and in-house investigations (3.1. and 3.2.), M.S., J.G., S.S. and P.K.; gas permeation test stand investigations (3.3.1.), K.W.; gas permeation pilot plant investigations (3.3.2.), M.S., P.K.; comparison of flue gas compositions at both power plants (3.4.), P.K.; Software, P.K.; Writing, P.K.; writing-review and editing, S.S., P.K., K.W.

Funding: This research was funded by the Helmholtz Association of German Research Centres through the Helmholtz Portfolio MEM-BRAIN.

Acknowledgments: The authors would like to acknowledge financial support from the Helmholtz Association of German Research Centres through the Helmholtz Portfolio MEM-BRAIN. The authors would like to thank the employees of EnBW AG in Karlsruhe, especially Christopher Blessing, Ludwig Herz and the laboratory staff as well as the employees of RWE AG in Niederaussem, especially Georg Wiechers and Peter Moser for practical and theoretical support at both investigation sites. We are also thankful for the support of Klaus Huber and Holger Dörr (DVGW Research Centre at Engler-Bunte-Institute (EBI) of Karlsruhe Institute of Technology (KIT)). The authors also like to thank Clarissa Abetz (Institute of Polymer Research) for SEM investigations.

Conflicts of Interest: The authors declare no conflict of interest.

References

1. Lashof, D.A.; Ahuja, D.R. Relative contributions of greenhouse gas emissions to global warming. *Nature* **1990**, *344*, 529. [CrossRef]
2. Ansolobehere, S.; Beer, J.; Deutch, J.; Ellerman, A.D.; Friedman, J.; Herzog, H.; Jacoby, H.; Joskow, P.; McRae, G.; Lester, R.; et al. *The Future of Coal—Options for a Carbon Constrained World, an Interdisciplinary MIT Study*; Massachusetts Institute of Technology: Cambridge, MA, USA, 2007.
3. Erneuerbare Energien. Available online: <https://www.bmwi.de/Redaktion/DE/Dossier/erneuerbare-energien.html> (accessed on 29 November 2017).
4. Pires, J.C.M.; Martins, F.G.; Alvim-Ferraz, M.C.M.; Simões, M. Recent developments on carbon capture and storage: An overview. *Chem. Eng. Res. Des.* **2011**, *89*, 1446–1460. [CrossRef]
5. Araújo, O.d.Q.F.; de Medeiros, J.L. Carbon capture and storage technologies: Present scenario and drivers of innovation. *Curr. Opin. Chem. Eng.* **2017**, *17*, 22–34. [CrossRef]
6. D’Alessandro, D.M.; Smit, B.; Long, J.R. Carbon dioxide capture: prospects for new materials. *Angew. Chem. Int. Ed.* **2010**, *49*, 6058–6082. [CrossRef] [PubMed]
7. Luis, P. Use of monoethanolamine (MEA) for CO₂ capture in a global scenario: Consequences and alternatives. *Desalination* **2016**, *380*, 93–99. [CrossRef]
8. Bushuyev, O.S.; De Luna, P.; Dinh, C.T.; Tao, L.; Saur, G.; van de Lagemaat, J.; Kelley, S.O.; Sargent, E.H. What Should We Make with CO₂ and How Can We Make It? *Joule* **2018**, *2*, 825–832. [CrossRef]
9. Brinkmann, T.; Lillepär, J.; Notzke, H.; Pohlmann, J.; Shishatskiy, S.; Wind, J.; Wolff, T. Development of CO₂ Selective Poly(Ethylene Oxide)-Based Membranes: From Laboratory to Pilot Plant Scale. *Engineering* **2017**, *3*, 485–493. [CrossRef]
10. Li, M.; Zhang, X.; Zeng, S.; Bai, L.; Gao, H.; Deng, J.; Yang, Q.; Zhang, S. Pebax-based composite membranes with high gas transport properties enhanced by ionic liquids for CO₂ separation. *RSC Adv.* **2017**, *7*, 6422–6431. [CrossRef]
11. Pilot Testing of a Membrane System for Postcombustion CO₂ Capture. Available online: <https://www.osti.gov/scitech/biblio/1337555> (accessed on 30 November 2017).
12. Plechkova, N.V.; Seddon, K.R. Applications of ionic liquids in the chemical industry. *Chem. Soc. Rev.* **2008**, *37*, 123–150. [CrossRef] [PubMed]
13. Walden, P. Molecular weights and electrical conductivity of several fused salts. *Bull. Acad. Imp. Sci. (St. Petersburg)* **1914**, *8*, 405–422.
14. Earle, M.J.; Esperanca, J.M.; Gilea, M.A.; Lopes, J.N.; Rebelo, L.P.; Magee, J.W.; Seddon, K.R.; Widegren, J.A. The distillation and volatility of ionic liquids. *Nature* **2006**, *439*, 831–834. [CrossRef] [PubMed]
15. Anderson, J.L.; Ding, R.; Ellern, A.; Armstrong, D.W. Structure and properties of high stability geminal dicationic ionic liquids. *J. Am. Chem. Soc.* **2005**, *127*, 593–604. [CrossRef] [PubMed]
16. Smiglak, M.; Reichert, W.M.; Holbrey, J.D.; Wilkes, J.S.; Sun, L.; Thrasher, J.S.; Kirichenko, K.; Singh, S.; Katritzky, A.R.; Rogers, R.D. Combustible ionic liquids by design: Is laboratory safety another ionic liquid myth? *Chem. Commun.* **2006**, *24*, 2554–2556. [CrossRef] [PubMed]

17. Ohno, H.; Yoshizawa, M.; Mizumo, T. Ionic Conductivity. In *Electrochemical Aspects of Ionic Liquids*; John Wiley & Sons: Hoboken, NJ, USA, 2005; pp. 75–81.
18. Grünauer, J.; Shishatskiy, S.; Abetz, C.; Abetz, V.; Filiz, V. Ionic liquids supported by isoporous membranes for CO₂/N₂ gas separation applications. *J. Membr. Sci.* **2015**, *494*, 224–233. [CrossRef]
19. Grünauer, J.; Filiz, V.; Shishatskiy, S.; Abetz, C.; Abetz, V. Scalable application of thin film coating techniques for supported liquid membranes for gas separation made from ionic liquids. *J. Membr. Sci.* **2016**, *518*, 178–191. [CrossRef]
20. Tome, L.C.; Marrucho, I.M. Ionic liquid-based materials: A platform to design engineered CO₂ separation membranes. *Chem. Soc. Rev.* **2016**, *45*, 2785–2824. [CrossRef] [PubMed]
21. Zhou, J.; Mok, M.M.; Cowan, M.G.; McDanel, W.M.; Carlisle, T.K.; Gin, D.L.; Noble, R.D. High-Permeance Room-Temperature Ionic-Liquid-Based Membranes for CO₂/N₂ Separation. *Ind. Eng. Chem. Res.* **2014**, *53*, 20064–20067. [CrossRef]
22. Dai, Z.; Noble, R.D.; Gin, D.L.; Zhang, X.; Deng, L. Combination of ionic liquids with membrane technology: A new approach for CO₂ separation. *J. Membr. Sci.* **2016**, *497*, 1–20. [CrossRef]
23. Wang, B.; Qin, L.; Mu, T.; Xue, Z.; Gao, G. Are Ionic Liquids Chemically Stable? *Chem. Rev.* **2017**, *117*, 7113–7131. [CrossRef] [PubMed]
24. Crosthwaite, J.M.; Muldoon, M.J.; Dixon, J.K.; Anderson, J.L.; Brennecke, J.F. Phase transition and decomposition temperatures, heat capacities and viscosities of pyridinium ionic liquids. *J. Chem. Thermodyn.* **2005**, *37*, 559–568. [CrossRef]
25. Froba, A.P.; Kremer, H.; Leipertz, A. Density, refractive index, interfacial tension, and viscosity of ionic liquids [EMIM][EtSO₄], [EMIM][NTf₂], [EMIM][N(CN)₂], and [OMA][NTf₂] in dependence on temperature at atmospheric pressure. *J. Phys. Chem. B* **2008**, *112*, 12420–12430. [CrossRef] [PubMed]
26. Buschatz, H.; Hicke, H.-G.; Paul, D.; Peters, G.; Scharnagl, N. Membranen aus Polyacrylnitril. EP 0840645A2, 13 May 1998.
27. Yave, W.; Car, A.; Wind, J.; Peinemann, K.V. Nanometric thin film membranes manufactured on square meter scale: Ultra-thin films for CO₂ capture. *Nanotechnology* **2010**, *21*, 395301. [CrossRef] [PubMed]
28. Mushardt, H.; Kramer, V.; Hülägü, D.; Brinkmann, T.; Kraume, M. Development of Solubility Selective Mixed Matrix Membranes for Gas Separation. *Chem. Ing. Tech.* **2014**, *86*, 83–91. [CrossRef]
29. Escorihuela, S.; Tena, A.; Shishatskiy, S.; Escolastico, S.; Brinkmann, T.; Serra, J.M.; Abetz, V. Gas Separation Properties of Polyimide Thin Films on Ceramic Supports for High Temperature Applications. *Membranes* **2018**, *8*, 16. [CrossRef] [PubMed]
30. Ohlrogge, K.; Wind, J.; Brinkmann, T.; Scheel, H.; Stegger, J.; Tiberi, T. 2.9 Progress in the Use of Membrane Technology to Separate Volatile Organic Compounds (VOCs). In *Comprehensive Membrane Science and Engineering*; Elsevier: Amsterdam, The Netherlands, 2017; pp. 226–255.
31. Brinkmann, T.; Pohlmann, J.; Withalm, U.; Wind, J.; Wolff, T. Theoretical and experimental investigations of flat sheet membrane module types for high capacity gas separation applications. *Chem. Ing. Tech.* **2013**, *85*, 1210–1220. [CrossRef]
32. Ohlrogge, K.; Ebert, K. *Membranen: Grundlagen, Verfahren und Industrielle Anwendungen*; Wiley-VCH: Weinheim, Germany, 2006.
33. Der Hochleistungswäscher REAplus. Available online: <http://www.rwe.com/web/cms/mediablob/de/254152/data/974594/4/rwe/innovation/kraftwerke/fossil-gefeuerte-kraftwerke/hochleistungswaescher-reapplus/Broschuere-Der-Hochleistungswaescher-REAplus.pdf> (accessed on 10 April 2018).
34. Pohlmann, J.; Bram, M.; Wilkner, K.; Brinkmann, T. Pilot scale separation of CO₂ from power plant flue gases by membrane technology. *Int. J. Greenh. Gas Control* **2016**, *53*, 56–64. [CrossRef]
35. Aspen Custom Modeler. Available online: <https://www.aspentech.com/en/products/pages/aspen-custom-modeler> (accessed on 14 March 2018).
36. Kabadı, V.N.; Danner, R.P. A modified Soave-Redlich-Kwong equation of state for water-hydrocarbon phase equilibria. *Ind. Eng. Chem. Process Des. Dev.* **1985**, *24*, 537–541. [CrossRef]
37. Zha, F.F.; Fane, A.G.; Fell, C.J.D.; Schofield, R.W. Critical displacement pressure of a supported liquid membrane. *J. Membr. Sci.* **1992**, *75*, 69–80. [CrossRef]
38. Moser, P.; Wiechers, G.; Stahl, K.; Stoffregen, T.; Vorberg, G.; Lozano, G.A. Solid Particles as Nuclei for Aerosol Formation and Cause of Emissions—Results from the Post-combustion Capture Pilot Plant at Niederaussem. *Energy Procedia* **2017**, *114*, 1000–1016. [CrossRef]

39. Moser, P.; Schmidt, S.; Stahl, K.; Vorberg, G.; Lozano, G.A.; Stoffregen, T.; Richter, T. The wet electrostatic precipitator as a cause of mist formation—Results from the amine-based post-combustion capture pilot plant at Niederaussem. *Int. J. Greenh. Gas Control* **2015**, *41*, 229–238. [[CrossRef](#)]
40. Saha, C.; Irvin, J.H. Real-time aerosol measurements in pilot scale coal fired post-combustion CO₂ capture. *J. Aerosol Sci.* **2017**, *104*, 43–57. [[CrossRef](#)]
41. Schaber, K. Aerosol formation in absorption processes. *Chem. Eng. Sci.* **1995**, *50*, 1347–1360. [[CrossRef](#)]
42. Li, Z.; Jiang, J.; Ma, Z.; Wang, S.; Duan, L. Effect of selective catalytic reduction (SCR) on fine particle emission from two coal-fired power plants in China. *Atmos. Environ.* **2015**, *120*, 227–233. [[CrossRef](#)]
43. Brachert, L.; Kochenburger, T.; Schaber, K. Facing the Sulfuric Acid Aerosol Problem in Flue Gas Cleaning: Pilot Plant Experiments and Simulation. *Aerosol Sci. Technol.* **2013**, *47*, 1083–1091. [[CrossRef](#)]
44. Merkel, T.C.; Lin, H.; Wei, X.; Baker, R. Power plant post-combustion carbon dioxide capture: An opportunity for membranes. *J. Membr. Sci.* **2010**, *359*, 126–139. [[CrossRef](#)]



© 2019 by the authors. Licensee MDPI, Basel, Switzerland. This article is an open access article distributed under the terms and conditions of the Creative Commons Attribution (CC BY) license (<http://creativecommons.org/licenses/by/4.0/>).